Aligned carbon nanotube/zinc oxide nanowire hybrids as high performance electrodes for supercapacitor applications

Ahmed S. Al-Asadi, Luke Alexander Henley, Milinda Wasala, Baleeswaraiah Muchharla, Nestor Perea-Lopez, Victor Carozo, Zhong Lin, Mauricio Terrones, Kanchan Mondal, Krisztian Kordas, and Saikat Talapatra

Carbon nanotube/metal oxide based hybrids are envisioned as high performance electrochemical energy storage electrodes since these systems can provide improved performances utilizing an electric double layer coupled with fast faradaic pseudocapacitive charge storage mechanisms. In this work, we show that high performance supercapacitor electrodes with a specific capacitance of ~192 F/g along with a maximum energy density of ~3.8 W h/kg and a power density of ~28 kW/ kg can be achieved by synthesizing zinc oxide nanowires (ZnO NWs) directly on top of aligned multi-walled carbon nanotubes (MWCNTs). In comparison to pristine MWCNTs, these constitute a 12-fold of increase in specific capacitance as well as corresponding power and energy density values. These electrodes also possess high cycling stability and were able to retain ~99% of their specific capacitance value over 2000 charging discharging cycles. These findings indicate potential use of a MWCNT/ZnO NW hybrid material for future electrochemical energy storage applications

I. INTRODUCTION

High performance, cost-effective, and environmentally friendly renewable energy storage devices are crucial in order to mitigate the present energy challenge.[1–4] Among various energy storage devices, electrochemical capacitors (ECs) or supercapacitors (SCs) are considered as one of the suitable options in order to develop energy efficient, robust, sustainable energy storage systems.[5,6] This is largely due to the fact that SCs exhibit longer life cycles and faster charge/discharge capability than conventional batteries.[7] In general, SC electrodes can be categorized into two groups, primarily based on charge storage mechanisms. These include (1) electrical double-layer capacitors (EDLCs), which employ the ion adsorption/desorption mechanism and typically use carbonbased materials as electrodes and (2) pseudocapacitors (PCs), which undergo rapid surface redox reactions that mainly involve transition metal oxides or electrically conductive pol-ymers as active electrode materials.[8] Carbon-based materials, such as multi-walled carbon nanotubes (MWCNTs), have been actively used as electrodes to fabricate EDLCs because these materials possess higher conductivity, higher chemical stability, larger specific surface area, and are lightweight.[9–11] Most of these properties are attributed due to the high aspect ratio of the MWCNTs and their nanoscopic sizes. The general advantages of the effects of nanostructuring the electrodes in electrochemical applications are well known.[12] However, using only carbon-based materials without much structural or chemical modification can restrict the SC performance.[13] In order to avoid this, researchers in the past have proposed several ways to incorporate various other nanostructures in order to synthesize carbon-based hybrid materials[14,15] that will have improved functionalities. In recent years, rational design of SC electrodes based on hybrids of

carbon nanotubes and transition metal oxide has received significant attention since these systems can utilize a combined charge storage phenomenon of electrochemical double layer as well as faradaic pseudocapacitive mechanisms.[16–20]

Several hierarchical and composite structures based on MWCNTs and transition metal oxides supercapacitor electro-des have been widely explored in order to impart significant component redox reaction in them. For example, various transition metal oxides, such as RuO_2,[16] In_2O_3,[17] V_2O_5,[18] ZnO,[19] and NiO,[20] have been successfully used to enhance the capacitive performance of MWCNTs by a few orders of magnitude higher compared to those of typical MWCNTs. Among these transition metal oxides, ZnO based materials have been utilized in many applications, such as light-emitting materials,[21,22] UV-sensors,[23] gas sensors,[24,25] solar cells,[26] and are also shown to have excellent performance as active batteryelectrode materials with a high energy density of 650 A/g.[27] Several investigations also indicate the possibility of using composites of carbon based materials and ZnO for energy applications such as CNT/ZnO[19,28] and graphene/ZnO[29] in order to fabricate a high performance supercapacitor.

In this work, we show a simple chemical bath deposition method (CBD) of fabricating a one-dimensional (1D) ZnO nanowire (NW) network on top of aligned MWCNTs. The fabricated MWCNT/ZnO NW structure showed very good electrochemical performance with a specific capacitance of ~192 F/g along with a maximum energy density of ~3.8 W h/kg and a power density of ~28 kW/kg. These electrodes also showed high cycling stability and were able to retain ~99% of their initial specific capacitance value after 2000 cycles. From the extensive circuit modeling/analysis performed on the information obtained from electrochemical impedance spectroscopy (EIS) analysis, it can be inferred that devices made out of these hybrids show very low equivalent series resistance (ESR) values of ~4 Ω. To the best of our knowledge, this study is the first to demonstrate the synthesis of 1-D ZnO on aligned MWCNTs by using a sequence of chemical vapor deposition (CVD)-CBD as electrodes for electrochemical energy-storage applications.

II. EXPERIMENTAL DETAILS

A. Reagents and materials

Hexamethylenetetramine (HMT), zinc nitrate hexahy-drate [$(Zn(NO_3)_2$ _ $6H_2O$], ferrocene [$C_{10}H_{10}Fe$, 99.9%], and xylene [C_8H_{10}, 99.9%] were purchased from Fisher Scientific Company and used without further purification or treatments. ZnO nanoparticles (NPs) with a diameter of approximately 20 nm were obtained from mkNANO.

B. Measurement tools

A FEI Quanta FEG 450 SEM system was used to investi gate the surface morphology of the MWCNT/ZnO NW hybrid. The SEM system was equipped with an energy dispersive spectroscopy (EDS) detector to investigate the energy spectrum and to determine the chemical composition of the materials. Raman spectroscopy was performed to provide further details on the MWCNT/ZnO NW structure. The Raman spectrum was obtained using a Renishaw InVia confocal Raman microscope with a 50_ objective lens and a laser excitation wavelength of 514 nm that provided a laser spot size of 2 lm. Raman measurement was performed at room temperature, and power was maintained at 1.5 mW. CurrentVoltage (CV) and galvanostatic charging/discharging meas-urements were conducted by using an advanced electrochemical

system (PARSTAT 2263 Princeton Applied Research) controlled by PowerSuite™ Software. Electrical impedance spectroscopy (EIS) was conducted by using the same system at a frequency ranging from 174 mHz to 0.1 MHz, with a potential amplitude of 10 mV without DC offset.

C. Electrode fabrication

1. Aligned MWCNT growth procedure

Aligned MWCNTs were grown on a silicon dioxide (SiO_2)/silicon (Si) substrate through the well-established air-assisted CVD ferrocene ($C_{10}H_{10}Fe$)/xylene(C_8H_{10}) method as mentioned in our previous publications.[30,31] In brief, a clean horizontal quartz tube with a length of 1.2 m and a diameter of 50 mm was purged with argon gas and slowly heated to 790 ◦C in an argon environment. A catalyst precursor and a carbon source solution were prepared by dissolving $C_{10}H_{10}Fe$ in C_8H_{10} to obtain a solution of 0.01 g/mL. The prepared solution was injected into the tube furnace by using a syringe pump at a constant rate of 12 mL/h. Iron particles produced from $C_{10}H_{10}Fe$ acted as catalyst particles, and carbon atoms were generated by dissociating the C-C and C–H bonds of C_8H_{10}. During the growth, argon (85%) and hydrogen (15%) gases were allowed to flow into the furnace tube at a flow rate of approximately 500 sccm. The low temperature at the end of the furnace tube was sufficient to vaporize the injected solution, and vapors were carried into the reaction zone via argon and hydrogen flow. A small amount of air (approximately 2.5 sccm) was mixed with the reaction environment to maintain the catalyst activity. Aligned MWCNTs grew on SiO_2/Si substrates, which were placed in the reaction zone. The length of the aligned MWCNTs was adjusted by controlling the feeding time of C_8H_{10}/$C_{10}H_{10}Fe$ solution. For this work, we typically used MWCNTs of ~500 lm. After a desired growth was completed, the furnace was turned off to cool down the quartz tube reactor to room temperature in the argon environment. We obtained an array of densely packed aligned MWCNTs on the SiO_2/Si substrate, which was similar to that described in our previous studies.[32,33]

2. Fabrication of the MWCNT/ZnO NW hybrid structure

For the synthesis of ZnO nanowires on top of the aligned MWCNT materials, we followed a CBD technique with a specific recipe, as mentioned in one of our previous publications.[34] In brief, a simple seeding technique was applied to create a thin film of ZnO NPs on top of the aligned MWCNT structures as an agent for the CBD route.[34] After the seed layer was deposited, two equimolar aqueous solutions based on HMT (0.025 M, 80 mL) and $Zn(NO_3)_2{\cdot}6H_2O$ (0.025 M, 80 mL) were used to synthesize ZnO NWs onto the MWCNT surface. Each solution was mixed separately on a stirring plate for 5 min to dissolve all-inclusive chemicals with DI water. Subsequently, both solutions were mixed together with a metal stirring rod for 20 min. The prepared solution was transferred to a 400 mL glass beaker, and the substrate was completely submerged in the solution. The top beaker was sealed with aluminum foil and wrapped with electrical tape to secure the chemical interaction. The whole assembly was placed in an oven preheated at approximately 95 ◦C for 16 h. After 16 h, the flask was removed from the oven, and the sample was washed with DI water and left to dry naturally under ambient conditions before it was subjected to characterization or measurements. During the CBD process, the control of the growth requires some parameters adjustment (e.g., the growth duration, the pH of the solution, the temperature of the growth, etc.) in order to achieve high quality ZnO

NWs evenly distributed on the entire substrate. We followed our previous recipe[34] of obtaining well-distributed ZnO NWs. We have found that a growth period of 16 h period results in uniform growth of ZnO NWs on the top of the aligned MWCNTs with an estimated 1 micrometer ZnO Layer thickness and with an average diameter of 40–50 nm. Here, we would like to add that increasing the growth duration beyond 16 h would increase the thickness of ZnO NWs. This will decrease the value of specific capacitance due to the decrease in specific surface area. Figure 1(a) illustrates the steps utilized during the fabrication process of MWCNT/ZnO NW hybrid electrodes.

III. RESULTS AND DISCUSSION

A. Material characterization

Figure 1(b) shows a typical SEM image of the top portion of aligned MWCNTs. Such aligned forests of MWCNTs were used as substrates to grow networks of ZnO nanowires on top of them. Figure 1(c) displays the SEM image of a similar MWCNT forest after the ZnO growth process was completed. Figure 1(c) specifically shows the cross section of the MWCNT/ZnO NW hybrid structure. A clear interface showing the aligned MWCNT forest and the ZnO NW is clearly observed. In Figure 1(d), the SEM image obtained from the top of the MWCNT surface after CBD of ZnO nanowires is shown. From the SEM image, it is clear that the nanowires grown on top of the MWCNT forest are evenly distributed on the surface of MWCNTs.

Further structural investigation on ZnO nanowires grown on top of MWCNTs was performed by Raman spectroscopy, as shown in Figure 1(e). Based on the group theory, the wurtzite ZnO belongs to the C^4_{6v} space group, which contains eight optical phonon modes at the C point of the Brillouin zone.[35,36] These modes can be defined as Raman active modes ($A_1 + E_1 + 2E_2$), Raman silent mode ($2B_1$), and infrared active modes ($A_1 + E_1$).[35,36] The $2E_2$ mode is divided into two active modes, namely, E_2 (high) and E_2 (low), which are associated with the vibration of the O and Zn atoms, respectively.[37] The infrared active modes ($A_1 + E_1$) is further split into two: transverse optical (TO) and longitudinal optical (LO) phonons. The vibrational modes obtained from our ZnO NWs are shown in Figure 1(e). The observed Raman shifts in our samples are assigned to $2E_2$ (333.4 cm^{-1}), A_1 (TO) (383.4 cm^{-1}), E_1 (TO) (413.3 cm^{-1}), E2 (high) (439.8 cm^{-1}), E_1 (LO) (580.4 cm^{-1}), A_1 (TO + LO) (1055.6 cm^{-1}), and $2E_1$ (LO) (1145.5 cm^{-1}). The existence of the $2E_2$ peak at ~333.4 cm^{-1} indicates that the grown ZnO NWs exhibit a strong crystalline order.[36] In addition, the dominant peak intensity of the E_2 (high) line at 438 cm^{-1} is a strong evidence that ZnO NWs have hexagonal wurtzite structures and oriented along the c-axis.[36] The presence of E_1 (LO) generally originates from impurities and/or defects, such as oxygen vacancies formed during the growth process.[38] The assigned peaks are consistent with the reported data of ZnO.[39]

B. Electrochemical measurements

After the completion of ZnO nanowire growth on top of the MWCNTs, the hybrid was removed from the SiO_2/Si substrate and used as an electrode to fabricate the SCs in parallel plate geometry. Two pieces of the MWCNT/ZnO NW electrode (0.25 cm x 0.25 cm) were sandwiched together, separated from each other by a filter paper (Whatman™), and subsequently transferred to a sealed stainless steel electrochemical cell (Model EQ-STC, MTI Corporation) with polished stainless steel current collectors. The electrochemical

performance of the MWCNT/ZnO NW SC was evaluated using standard techniques of cyclic voltammetry (CV), charge discharge (CD) cycles, as well as electrochemical impedance spectroscopy (EIS). CV characterizations were performed at various scan rates ranging from 1 mV/s to 200 mV/s by using 6M potassium hydroxide (KOH) as an electrolyte. Figure 2(a) shows the excellent CV responses obtained using the MWCNT/ZnO NW electrodes. We would like to note here that unlike some of the previous reported CV studies on ZnO based supercapacitors[19,28] which showed clear redox peaks, the CVs in this study are nearly rectangular at all the scan rates. The near rectangular CV curves even at high scan rates indicate a good capacitive behavior of these electrodes and a fast charging– discharging process. The absence of these peaks is related to a coupled effect of synchronization of a double layer and redox reactions.[40–42] According to Saranya et al.,[43] the possible faradaic reactions are

$$ZnO + OH^- \leftrightarrow ZnOOH + e^-. \quad (1)$$

On the other hand, Shi et al.[44] and Venugopal et al.[45] have stated that the following reactions are likely:

$$ZnO + K^+ + e^- \leftrightarrow ZnOK. \quad (2)$$

Ideal capacitors based on the charge storage result in rectangular CVs. Pseudocapacitance on the other hand is faradic in nature and thus does not result in perfect rectangular CVs but at the same time is not and should not be related to redox peaks. The redox peaks occur when the redox active sites are isolated either due to the nature of their distribution or due to poor conductivity between the electrode and the collector. However, the redox peaks may not be observable for a variety of reasons including (a) the redox reactions are fast and reversible, (b) the redox sites are electrically coupled due to good electrical conductivity, (c) short separations, and (d) the availability of the majority of the sites on the surface to circumvent solid ion diffusion. Under these conditions, the hybrid electro-des are charged and discharged rapidly at pseudo-constant rates over the entire voltammetric cycle, resulting in the absence of peaks. It should also be noted that Faradaic peaks become clear if the double layer is weak. However, in the case of good electric double layer (EDL) capacitance along with high electrode material utility due to high specific surface areas (as in porous structures), the reaction peak becomes broad and weak. We attribute the observed non-redox peak CV seen for ZnO NWs grown on top of aligned MWCNTs to their unique compositional structure of these hybrids that meets several of the above-mentioned criteria. The ZnO nanowire structure ensures that the majority of the redox sites is available and is present on the nanowire surface. The structure not only increases the wettable surface area but also improves the conductivity due to the aligned 1-D structure of the nanowire. The aligned nanotube –nanowire hybrid structure facilitates fast electron transfer between the electrode and the collector and the ZnO nanowires allow faster charge discharge rates as the faradaic reaction replaces the diffusion-controlled $K^þ$ion intercalation process. In order to verify that alignment of CNTs plays a significant role in the electrochemical performance of CNT-ZnO composites, we measured CNT-ZnO composite devices, where ZnO nanowires were grown on CNT buckypaper (network of unaligned CNTs-data not shown). We have tested two devices based on ZnO/CNT buckypaper using 6M KOH as the electrolyte. We found that both these devices show a specific capacitance several orders of magnitude less (around 9 F/g at scan rate of 10 mV/s) for the first device and (9.6 F/g at scan rate of 5 mV/s) for the second device than those reported for the aligned ZnO-CNT composite. All these above attributes of the hybrid

structure perhaps result in excellent electrochemical performance as indicated by near rectangular CVs. In addition, NWs can present transport channels for more electrical charges to be stored and transferred to the electrodes. Similar observations were observed to some extent by other researchers.[19,43,46] The specific capacitance C_{sp} was calculated from the CV curves by using the following relation:

$$C_{sp} = 2\int idV/smΔV, \quad (3)$$

where the integral refers to the area of the CV curve, s represents the scan rate of each individual curve, m denotes the mass of a single electrode, and DV symbolizes the potential window. Figure 2(b) shows the calculated values of C_{sp} as a function of scan rate for the MWCNT/ZnO NW hybrid electrode. The highest C_{sp} = 192 F/g was achieved at scan rates of 1 mV/s. For comparison, specific capacitance measurements performed on as produced MWCNTs electrodes utilizing a similar procedure were found to be ~16 F/g. This indicates that the value of C_{sp} obtained for the hybrid electrode is an order of magnitude higher (~12 times more) than that of the as produced MWCNTs (Figure 2(b)). Figure 2(c) displays the galvanostatic charge/discharge (CD) curves collected at several different constant current densities. A negligible IR drop (0.84–1.3 mV) in these CD cycles further indicates a good electrical conductivity of the MWCNT/ZnO NW electrode.[47] Figure 2(d) illustrates that the specific capacitance of the device remains at approximately 99% of the initial value after 2000 charge/ discharge cycles, illustrating an excellent long-term cycling stability of these electrodes. The cycling stability of the CD measurements of MWCNT/ZnO NW electrodes over charge/discharge cycles is shown in the inset of Figure 2(d).

In order to evaluate the performance of MWCNT/ZnO NW supercapacitor electrodes, measurements were carried out for generating the Ragone plot. In Figure 3, the maximum energy density and power density obtained for a specific device are shown in a Ragone Plot. Energy density (ED) is evaluated using the following equation:

$$ED\left(\frac{Wh}{kg}\right) = C^2/2m', \quad (4)$$

where C is the charge/discharge capacitance, m' is the mass of both electrodes, and V denotes the potential window. Power density (PD) is calculated using the following equation:

$$PD\left(\frac{W}{kg}\right) = IV/m', \quad (5)$$

where I is the charge/discharge current. Typical devices showed that a maximum energy density of ~3.8 W h K^{-1} can be achieved using these hybrid electrodes.

In Table I, we have summarized our results and compared the performances of the MWCNT/ZnO NW supercapacitor devices with previously reported devices based on MWCNTs and MWCNT/metal oxide composites. The comparison is provided mainly in order to give a broad overview regarding the typical values that are obtained in the past on MWCNT/metal oxide based supercapacitor electrodes and to put into perspective the results obtained in this study. The maximum specific capacitance achieved for the MWCNT/ ZnO NW electrode (192 F/g) is about 12-fold higher than the maximum specific capacitance of pristine MWCNTs (16.6 F/ g; Table I) and 1.5-fold to 7-fold higher than those of MWCNTs/other metal oxides (24–166 F/g; Table I). We also note that while the power densities obtained in our devices are similar to several other MWCNT/metal oxide based composites the energy density is an order of magnitude less than some of the composites studied in the past such as TiO_2/ MWCNTs, RuO_2/MWCNTs, etc.[48] To illustrate, the equivalent series resistance R limits the PD values of electrochemical capacitors. Since the fabricated electrode in our experiment showed a low resistance (see the IR drop and EIS measurement) due to the high conductivity of highly crystal-line ZnO NWs, the obtained PD in this device was higher than all reports except Au-MnO_2/MWCNT, which showed a slightly higher PD due to the existence of Au particles which led to increase the conductivity of this electrode. In addition, increasing and/or decreasing the energy density of the electrode is related directly to the type of the electrolyte used to fabricate the electrochemical supercapacitor. The value of ED is typically prepositional to V^2 and C (Eq. (4)). In our experiment, we used 6M KOH which allows only 1 V window. The improvement of the ED value compared with old reports on (Pristine MWCNTs and CoOx/MWCNTs), which used a similar electrolyte (6M KOH), is mainly due to the high specific capacitance values observed in our experiments. But when we compare our results with RuO_2/MWCNT, TiO_2/MWCNT, and SnO_2/MWCNT, we found that their ED results are much higher due to the use of the 2M H_2SO_4 electrolyte which allowed a higher voltage window of 1.8 V. This could clearly explain the reason of obtaining a lower ED in our system compared to past reports.

In order to further understand and analyze the electrochemical processes occurring in our devices, we have performed electrochemical impedance spectroscopy of one of our devices (Figure 4). Figures 4(a) and 4(b) display the Nyquist plot, which shows the frequency response of the SC device. The Nyquist plot shows a semi-circle arc in a high-frequency region, which originates from the charge transfer of the double-layer capacitor and redox reaction at the electrode/electrolyte interface.[51] The intercept of the high-frequency region with the real impedance is typically used to determine the equivalent series resistance (ESR) of the device.[52] The ESR is a combination of the electrolyte, electrode material, and interfacial resistance.[53] The ESR value obtained for this particular device was found to be approximately ~4.2 Ω, (Figure 4(b)) which is comparable with 7, 4, 3, and 5.5 Ω as measured on pure MWCNT, RuO_2/ MWCNT, TiO_2/MWCNT, and SnO_2/MWCNT nanocomposite electrodes, respectively.[48,49] At a low frequency, the impedance shows a straight line with an acute angle between 45° and 90°, which is a real impedance. This line represents the diffusion of ions in the MWCNT/ZnO NW electrode. The deviation of the angle in this line from 45° is typically caused by the porous nature of the electrode surface.[54]

The impedance spectrum was fitted with a simple equivalent circuit (Figure 4(c)) over the whole range of measurement. The components of the equivalent circuit included the equivalent circuit resistance R_1, the resistance due to the redox reactions at the electrode/electrolyte interface, R_2, a constant phase element (CPE) component, which manifests the double layer capacitance of the system, a Warburg diffusion element component along with another capacitive component C, representing the pseudocapacitance contribution. Values of these components were extracted from the fitting in order to further understand the physical processes occurring in the MWCNT/ZnO NW electrode system.[55,56] The value of R_1 acquired from the fitting

is 4.0 Ω, which is consistent with the experimental data. The CPE, which yields the double-layer capacitance, can be calculated from the following equation:

$$C_{CPE} = P/\left[\omega^{1-n} sin\left(\frac{n\pi}{2}\right)\right], \qquad (6)$$

where P and n are fitting parameters (Table II) and ω=2πf. The Warburg element (W) represents the diffusion of ions into the electrode.[56] The presence of the C element, which is attributed to the contribution of the pseudocapacitance in the system, was also obtained from the fitting. The fitting parameters and the values of different components obtained from the fitting of the EIS measurement are shown in Table II. From the extracted data, it is important to note that the contribution of the CPE component in this system is ~2.6 x 10^{-5} F, whereas the pseudocapacitance contribution is ~20.7 x 10^{-5} F. This indicates that the double layer contribution to the total capacitance is ~11%, whereas the pseudocapacitance contribution is ~89% of the total capacitance. Further, the value of the pseudocapacitance is ~8 times greater than the double layer capacitance (manifested through CPE). This increase is similar to the increase in C_{sp} values (~12 times) of aligned MWCNT/ZnO NW electrodes when compared with pristine MWCNT electrodes. This further signifies the role of the ZnO NW's in enhancing the capacitive values of the EDLC through pseudocapacitive contribution.

IV. CONCLUSIONS

In conclusion, we have shown that simply growing ZnO nanowires on top of aligned MWCNTs can provide significant improvements in their electrochemical charge storage behavior. In the past, it has been shown that such performan-ces can be further tuned by adjusting the ratio of the MWCNT and ZnO in the composite. For example, for a given composite material, the ratio seems to have an optimal value for the best electrochemical performances. We believe that similar behavior can be expected in our case as well. We are conducting such studies and the results will be published subsequently.[57,58] We have also noticed that during repeated electrochemical measurements, assembling the electrochemical cells as well as long cycling their performance does not chance drastically or abruptly. This indicates that robust mechanical structure of the electrodes, specifically needed for electrochemical storage application can be formed using this method. Further, these experimental results also indicate the importance of the pseudocapacitive component offered by the metal oxide nanostructures, when coupled with carbon based materials. The aligned MWCNT/ZnO hybrid electrode structure investigated also shows that the aligned carbon nano-tube structures present in these hybrid systems provide favorable conductive path, resulting in low equivalent series resistances of the supercapacitor devices. Low equivalent series resistance in turn improves the overall electrode performance. The electrochemical measurements indicate that the wettability of the electrolyte must be good. There are two reasons for this: (1) The ZnO nano structuring should make the surface hydrophobic and will deteriorate electrochemical performance of the electrodes. Such behavior is not observed in our experiments and (2) proper charge transfer (through CV measurements) as well as low ESR values indicates good wettability of the electrolyte/electrode interface. The investigations presented here therefore suggest the potential use of a combination of aligned carbon nanotubes and metal oxide nanostructures for high performance electrochemical energy storage device applications.

ACKNOWLEDGMENTS

A.S.A is thankful for the financial support from Higher committee for educational development in Iraq (HCED-IRAQ). ST and KM would like to acknowledge NSF Grant No. 1133143 for partial support of this work. ST would also like to acknowledge NSF Grant No. 1623238 for partial support of this work.

REFERENCES

[1]L. Craco and J. Faria, J. Appl. Phys. 119, 085107 (2016).

[2]M. A. I. Shuvo, G. Rodriguez, M. T. Islam, H. Karim, N. Ramabadran, J. C. Noveron, and Y. Lin, J. Appl. Phys. 118, 125102 (2015).

[3]A. Orphanou, T. Yamada, and C. Y. Yang, J. Appl. Phys. 119, 214311 (2016).

[4]A. K. Singh and K. Mandal, J. Appl. Phys. 117, 105101 (2015).

[5]X. Zang, P. Li, Q. Chen, K. Wang, J. Wei, D. Wu, and H. Zhu, J. Appl. Phys. 115, 024305 (2014).

[6]A. Mishra and S. Ramaprabhu, J. Appl. Phys. 112, 104315 (2012).

[7]J. Chen, N. Xia, T. Zhou, S. Tan, F. Jiang, and D. Yuan, Int. J. Electrochem. Sci. 4, 1163 (2009).

[8]S. Boukhalfa, K. Evanoff, and G. Yushin, Energy Environ. Sci. 5, 6872 (2012).

[9]C.-T. Hsieh, Y.-C. Chen, Y.-F. Chen, M. M. Huq, P.-Y. Chen, and B.-S. Jang, J. Power Sources 269, 526 (2014).

[10]Y. Zhu, H. I. Elim, Y.-L. Foo, T. Yu, Y. Liu, W. Ji, J.-Y. Lee, Z. Shen, A. T.-S. Wee, and J. T.-L. Thong, Adv. Mater. 18, 587 (2006).

[11]C. Du, J. Yeh, and N. Pan, Nanotechnology 16, 350 (2005).

[12]S. Chen, Y. Liu, and J. Chen, Chem. Soc. Rev. 43, 5372 (2014).

[13]R. A. Fisher, M. R. Watt, and W. J. Ready, ECS J. Solid State Sci. Technol. 2, M3170 (2013).

[14]M. Ho, P. Khiew, D. Isa, T. Tan, W. Chiu, and C. H. Chia, Nano 9, 1430002 (2014).

[15]S. W. Lee, J. Kim, S. Chen, P. T. Hammond, and Y. Shao-Horn, ACS Nano 4, 3889 (2010).

[16]J. H. Park, J. M. Ko, and O. O. Park, J. Electrochem. Soc. 150, A864 (2003).

[17]P.-C. Chen, G. Shen, S. Sukcharoenchoke, and C. Zhou, Appl. Phys. Lett. 94, 043113 (2009).

[18]Z. Chen, V. Augustyn, J. Wen, Y. Zhang, M. Shen, B. Dunn, and Y. Lu, Adv. Mater. 23, 791 (2011).

[19]L. Aravinda, K. Nagaraja, H. Nagaraja, K. U. Bhat, and B. R. Bhat, Electrochim. Acta 95, 119 (2013).

[20]P. Lin, Q. She, B. Hong, X. Liu, Y. Shi, Z. Shi, M. Zheng, and Q. Dong, J. Electrochem. Soc. 157, A818 (2010).

[21]T. Pauport e, O. Lupan, B. Viana, L. Chow, and M. Tchernycheva, in Controlling the Properties of Electrodeposited ZnO Nanowire Arrays for Light Emitting Diode, Photodetector and Gas Sensor Applications

(International Society for Optics and Photonics, 2014), p. 89871R.

[22]J. Hassan, M. Mahdi, Y. Yusof, H. Abu-Hassan, Z. Hassan, H. Al-Attar, and A. Monkman, Opt. Mater. 35, 1035 (2013).

[23]J. Hassan, M. Mahdi, S. Kasim, N. M. Ahmed, H. A. Hassan, and Z. Hassan, Mater. Sci.-Poland 31, 180 (2013).

[24]J. Guo, J. Zhang, M. Zhu, D. Ju, H. Xu, and B. Cao, Sens. Actuators, B 199, 339 (2014).

[25]J. Hassan, M. Mahdi, C. Chin, H. Abu-Hassan, and Z. Hassan, Sens. Actuators, B 176, 360 (2013).

[26]M. McCune, W. Zhang, and Y. Deng, Nano Lett. 12, 3656 (2012).

[27]M. Selvakumar, D. K. Bhat, A. M. Aggarwal, S. P. Iyer, and G. Sravani, Physica B 405, 2286 (2010).

[28]Y. Zhang, X. Sun, L. Pan, H. Li, Z. Sun, C. Sun, and B. K. Tay, Solid State Ionics 180, 1525 (2009).

[29]X. Li, Z. Wang, Y. Qiu, Q. Pan, and P. Hu, J. Alloys Compd. 620, 31 (2015).

[30]X. Zhang, A. Cao, B. Wei, Y. Li, J. Wei, C. Xu, and D. Wu, Chem. Phys. Lett. 362, 285 (2002).

[31]X. Li, X. Zhang, L. Ci, R. Shah, C. Wolfe, S. Kar, S. Talapatra, and P. M. Ajayan, Nanotechnology 19, 455609 (2008).

[32]S. Talapatra, S. Kar, S. Pal, R. Vajtai, L. Ci, P. Victor, M. Shaijumon, S. Kaur, O. Nalamasu, and P. Ajayan, Nat. Nanotechnol. 1, 112 (2006).

[33]R. Shah, X. Zhang, and S. Talapatra, Nanotechnology 20, 395202 (2009).

[34]A. S. Al-Asadi, L. A. Henley, S. Ghosh, A. Quetz, I. Dubenko, N. Pradhan, L. Balicas, N. Perea-Lopez, V. Carozo, and Z. Lin, J. Appl. Phys. 119, 084306 (2016).

[35]L.-L. Yang, J.-H. Yang, D.-D. Wang, Y.-J. Zhang, Y.-X. Wang, H.-L. Liu, H.-G. Fan, and J.-H. Lang, Physica E 40, 920 (2008).

[36]R. Yousefi and A. Zak, Mater. Sci. Semicond. Process. 14, 170 (2011).

[37]R. Zhang, P.-G. Yin, N. Wang, and L. Guo, Solid State Sci. 11, 865 (2009).

[38]J.-H. Park, J. Kim, Y. Kim, B.-T. Lee, S.-J. Jang, C.-K. Moon, and H.-J. Song, Appl. Phys. Lett. 83, 1989 (2003).

[39]R. Cusco, E. Alarcon-Llado, J. Ibanez, L. Artus, J. Jim enez, B. Wang, and M. J. Callahan, Phys. Rev. B 75, 165202 (2007).

[40]M. Selvakumar and D. K. Bhat, Appl. Surf. Sci. 263, 236 (2012).

[41]M. Yang, Y. Zhong, J. Bao, X. Zhou, J. Wei, and Z. Zhou, J. Mater. Chem. A 3, 11387 (2015).

[42]M. Selvakumar and D. Krishna Bhat, J. Appl. Polym. Sci. 107, 2165 (2008).

[43]M. Saranya, R. Ramachandran, and F. Wang, J. Sci.: Adv. Mater. Devices 1, 454 (2016).

[44]S. Shi, X. Zhuang, B. Cheng, and X. Wang, J. Mater. Chem. A 1, 13779 (2013).

[45]N. Venugopal, B. Yang, and T. Ko, Mater. Res. Innovations 16, 96 (2012).

[46]Z. Li, Z. Zhou, G. Yun, K. Shi, X. Lv, and B. Yang, Nanoscale Res. Lett. 8, 473 (2013).

[47]P. Yang, X. Xiao, Y. Li, Y. Ding, P. Qiang, X. Tan, W. Mai, Z. Lin, W. Wu, and T. Li, ACS Nano 7, 2617 (2013).

[48]A. L. M. Reddy and S. Ramaprabhu, J. Phys. Chem. C 111, 7727 (2007).

[49]A.-R. Rautio, O. Pitk€anen, T. J€arvinen, A. Samikannu, N. Halonen, M. Mohl, J.-P. Mikkola, and K. Kordas, J. Phys. Chem. C 119, 3538 (2015).

[50]A. L. M. Reddy, M. M. Shaijumon, S. R. Gowda, and P. M. Ajayan, J. Phys. Chem. C 114, 658 (2009).

[51]T. Zhai, X. Lu, Y. Ling, M. Yu, G. Wang, T. Liu, C. Liang, Y. Tong, and Y. Li, Adv. Mater. 26, 5869 (2014).

[52]R. K€otz, M. Hahn, and R. Gallay, J. Power Sources 154, 550 (2006).

[53]Y. Yang, L. Li, G. Ruan, H. Fei, C. Xiang, X. Fan, and J. M. Tour, ACS Nano 8, 9622 (2014).

[54]A. Sharifi-Viand, M. Mahjani, and M. Jafarian, J. Electroanal. Chem. 671, 51 (2012).

[55]X. Liu, K. Liu, W. Zhou, L. Li, K. Zhou, and S. Chen, Sci. Adv. Mater. 7, 2336 (2015).

[56]W. Wang, S. Guo, I. Lee, K. Ahmed, J. Zhong, Z. Favors, F. Zaera, M. Ozkan, and C. S. Ozkan, Sci. Rep. 4, 4452 (2014).

[57]J. S. Suroshe and S. S. Garje, J. Mater. Chem. A 3, 15650 (2015).

[58]Y. Zhang, X. Sun, L. Pan, H. Li, Z. Sun, C. Sun, and B. K. Tay, J. Alloys Compd. 480, L17 (2009).

FIGURES AND TABLES

TABLE I. A comparative tabulation of the specific capacitance, energy density, and power density of MWCNT metal oxide based supercapacitor electrode materials.

Electrode material	Electrolyte	Maximum C_{sp} (F/g)	PD (kW/kg)	ED (Wh/kg)	Ref.
Pristine MWCNTs	6M KOH	16,6	…	0.58	49
CoOx/MWCNTs	6M KOH	24	…	0.86	49
In_2O_3 NW/MWCNT	Non-aqueous	64	7.48	1.29	17
RuO_2/MWCNT	1 M H_2SO_4	147	0.5	36.8	48
TiO_2/MWCNT	1 M H_2SO_4	166	0.5	40.2	48
SnO_2/MWCNT	1 M H_2SO_4	98	0.5	25	48
MnO_2/MWCNT	0.1 M Na_2SO_4	44	11	2.9	50
Au-MnO_2/MWCNT	0.1 M Na_2SO_4	68	33	4.5	50
MWCNT	6M KOH	16	N/A	N/A	This work
MWCNT/ZnO NW	6M KOH	192	~28	~3.8	This work

TABLE II. Fitting parameter of EIS spectrum.

Parameter	Value
C(F)	20.7×10^{-5}
$R_1(\Omega)$	4.0
$R_2(\Omega)$	15.63
W	24.81
P	8.3×10^{-5}
n	0.8
C_{CPE}(F)	2.6×10^{-5}
C_{Total}(F)	23.3×10^{-5}

FIG. 1. (a) Schematic of the fabrication process of the MWCNT/ZnO NW hybrid structure. (b) Cross-sectional SEM image showing the MWCNTs before ZnO NW growth. (c) ZnO NWs grown on MWCNTs. (d) SEM image showing the top of MWCNTs compactly covered by ZnO NWs. (e) Raman spectrum of ZnO NWs, including the experimental data and Gaussian–Lorentzian peak fitting; the inset magnifies the range of 200–500 cm^{-1}.

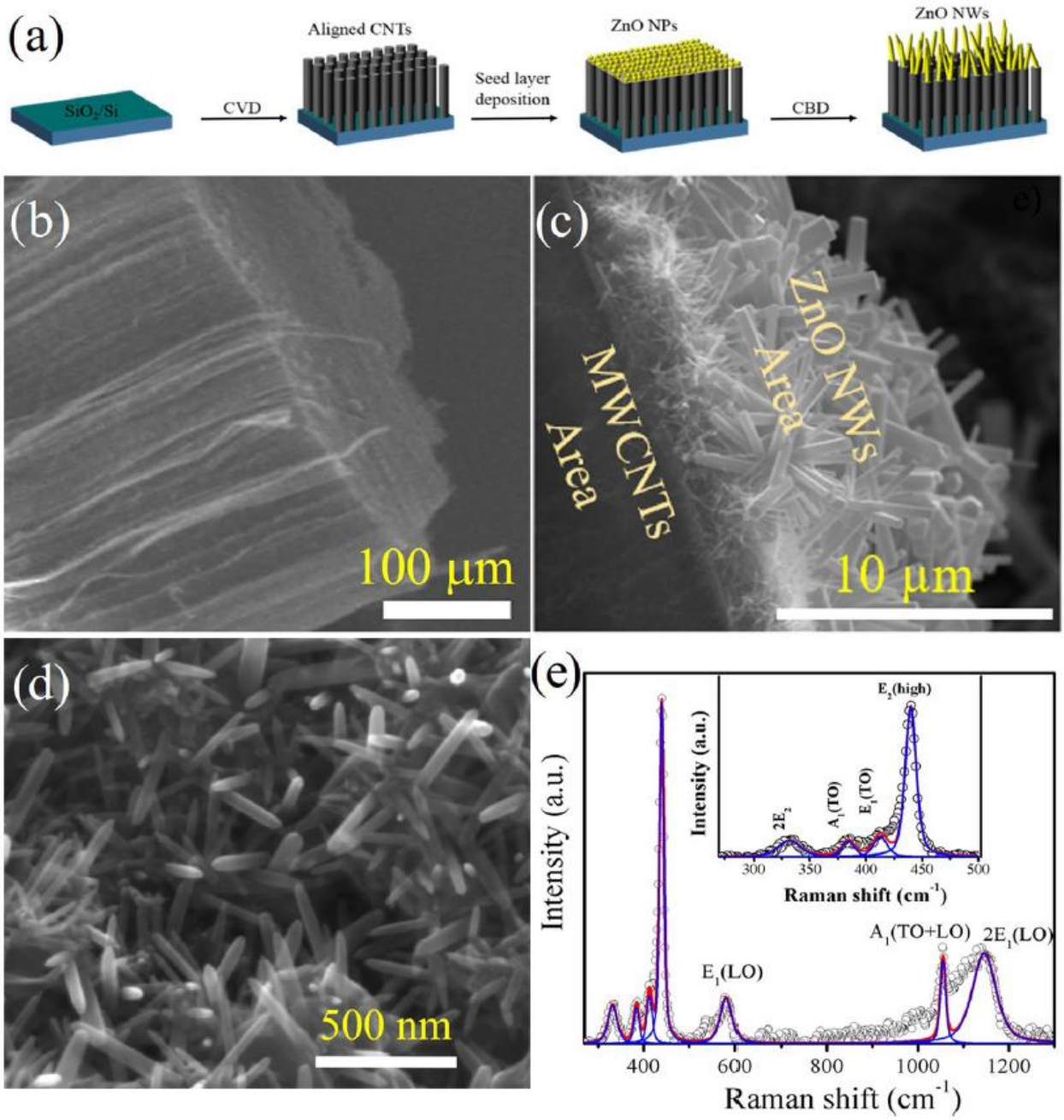

FIG. 2. (a) CV of the MWCNT/ZnO NW electrode at different scan rates: 1, 10, 30, 50, and 200 mV/s. (b) Specific capacitance of the as-prepared MWCNT/ ZnO NW and MWCNT electrodes by using 6M KOH as an electrolyte at different scan rates. (c) Charge/discharge curves of the MWNCT/ZnO NW electrode at different current densities. (d) Percent capacitance retained by MWCNT/ZnO NW for 2000 cycles.

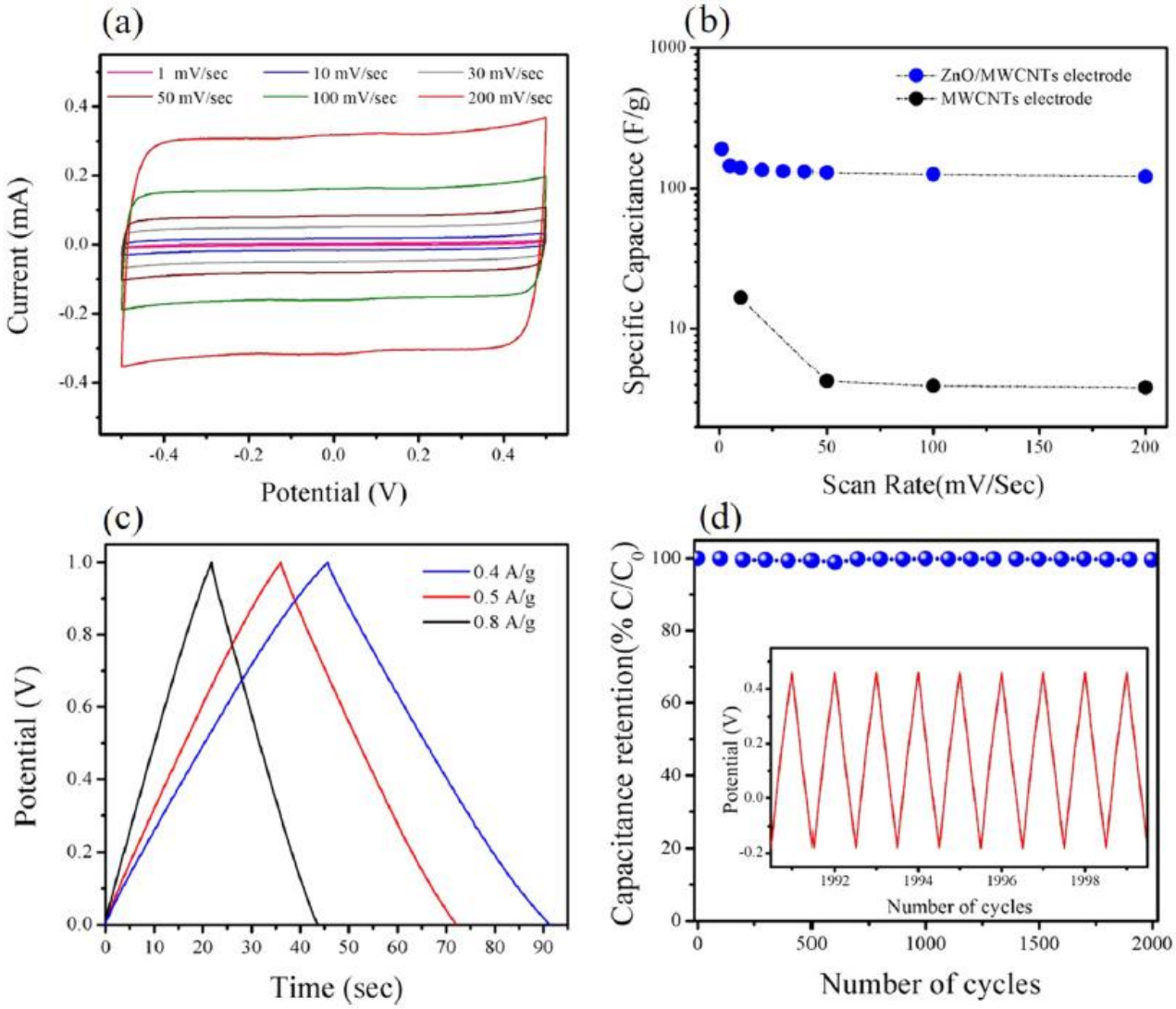

FIG. 3. Ragone plot of the MWCNT/ZnO NW hybrid structure.

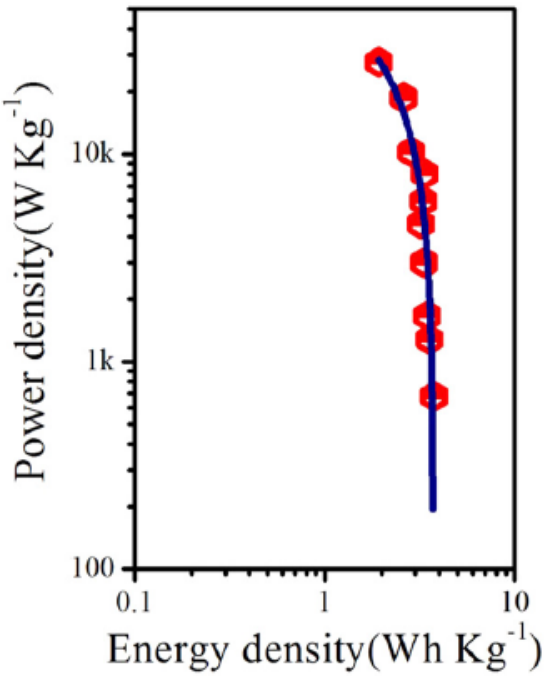

FIG. 4. (a) Electrochemical impedance spectroscopy (EIS) of the MWCNT/ ZnO NW electrode showing the experimental and fitted data. (b) High-frequency range showing the semi-cycle and intercept with real impedance. (c) Equivalent circuit model used for EIS fitting.